

# On Rayleigh-Bénard Mechanism of Alignment of Salt Fingers in Reactive Immiscible Two-Layer Systems

Dmitry A. Bratsun

Received: 19 December 2013 / Accepted: 27 May 2014 / Published online: 8 June 2014  
© Springer Science+Business Media Dordrecht 2014

**Abstract** The stability of a front of chemoconvective finger structures being spontaneously formed in a two-layer system of fluids filling a vertical Hele-Shaw cell, each of them containing a reactant of an exothermic  $A + B \rightarrow S$  reaction is examined. If the configuration consists of more dense acid (or salt) on top of less dense base in the presence of gravity, the development of the Rayleigh-Taylor instability leads to the standard scenario of density fingering. Despite the widespread perception of fingering as an irregular process, we show that, at least in some cases, the exact balance between the instabilities involved can result quasi-regular fingering pattern formation. In the case of immiscible fluids, we demonstrate that the Rayleigh-Bénard mechanism associated with intensive heat release during the reaction performs fine-tuning of the envelope of salt fingers. The mathematical model we develop consists in a set of reaction-diffusion-convection equations governing the evolution of concentrations and temperature coupled to Navier-Stokes and energy equations, written in a Hele-Shaw approximation. The results of linear stability analysis and direct numerical simulations of the fully nonlinear system are presented.

**Keywords** Chemo-hydrodynamics · Two-phase systems · Pattern formation · Convection · Fingering

## Introduction

Hydrodynamic instabilities arising near the interface between two or more immiscible liquids occur in a number of important technological applications (Nepomnyashchy et al. 2012). In many cases these processes are accompanied with exothermic chemical reactions at the interface or near it. Over the last few decades binary liquid-liquid systems with a chemical reaction have been the subject of increased fundamental investigations of the interaction between reaction-diffusion phenomena and pure hydrodynamic instabilities. In such systems, the instability of the fluid interface may generate local convective fluxes and thereby markedly affect the reaction as well as the interface heat and mass transfers. In these cases, self-organization processes may lead to a specific dissipation pattern formation of chemo-hydrodynamic nature.

Probably the first experimental evidence of convective mass transfer accompanied by chemical reaction in liquid-liquid systems was obtained by Quincke (1888) who observed spontaneous emulsification when a solution of lauric acid in oil is brought in contact with an aqueous solution of  $NaOH$ .

More recently (Sherwood and Wei 1957) observed spontaneous turbulence in the extraction of acetic acid from an organic solvent into an alkaline solution and acceleration of the interfacial reaction by convection. Dupeyrat and Nakache (1978) also observed interfacial turbulence related to the reaction of an alkyl ammonium ion with picric acid at an oil-aqueous interface. It is not clear how the processes in the bulk of liquid influenced the mass transfer in these cases. But Berg and Morig (1969) gave the experimental evidence that density gradients developed during the transfer of a solute across a liquid-liquid interface exert a strong influence on convection generated by interfacial

D.A. Bratsun (✉)  
Theoretical Physics Department, Perm State Humanitarian Pedagogical University, Ulitsa Sibirskaya 24, 614990 Perm, Russia  
e-mail: dmitribratsun@rambler.ru

tension variations. The convective motions were reported not to be localized near the interface but stream away from the interface and penetrating deeply into the bulk phases.

Another example of chemo-convective mass transfer was given by Avnir and Kagan (1995) who have studied pattern formation at liquid-gas interfaces driven by photochemical reactions. One more experimental example was given by Pons et al. (2000) who have fixed the convective instability in a thin fluid layer due to the increase of fluid density in the subsurface layer caused by the  $O_2$  oxidation of glucose to gluconic acid with the methylene blue as a catalyst.

For simple, irreversible chemical schemes such as an exothermic neutralization reaction  $A + B \rightarrow S$ , it has been shown that heat and solutal effects due to the reaction interplaying with a liquid-liquid interface and convection may result in a novel type of instability occurring when an organic solvent with a carboxylic acid is in contact with an aqueous solution of an inorganic base (sodium hydroxide) (Eckert and Grahn 1999). The self-sustained dynamics and pattern formation in the form of irregular plumes and fingers were shown to originate from the coupling between different gravity-dependent hydrodynamic instabilities such as Rayleigh-Taylor, diffusive-layer convection, Rayleigh-Bénard, Marangoni and double diffusive instabilities (Trevelyan et al. 2011; Bratsun and De Wit 2011).

In experimental work (Eckert et al. 2004), new effects have been discovered in the same system when non-organic base was replaced by an organic one. It has been found that one can obtain different structures by varying the types of reactants and their initial concentrations. Among these structures, a periodic set of chemoconvective fingers with one side keeping contact with the interface and the other side propagating in the direction out of the interface appears with an intriguing regularity (Fig. 1).

It should be noted that reactive fingering is well known in nonlinear chemistry, but evolving structures are usually

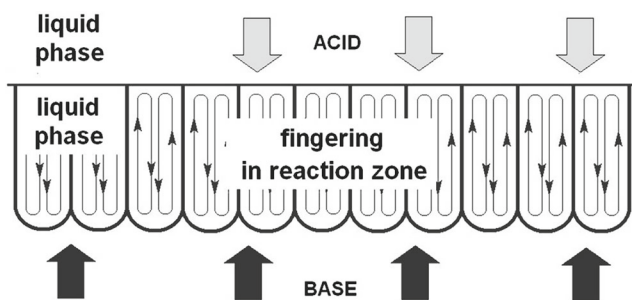


**Fig. 1** Schematic representation of transfer processes in the reactive immiscible system

chaotic. For example, all the works devoted to the case of miscible fluids usually state the formation of irregular patterns of fingers (De Wit 2001; Almarcha et al. 2010; Almarcha et al. 2011). For example, recently Almarcha et al. (2011) have shown that the various possible convective regimes can be triggered by acid-base reactions when a less dense acid solution ( $HCl$ ) lies on top of a denser alkaline one ( $NaOH$ ) in the gravity field. The possible dynamics are a composition of only two asymptotic cases: irregular plumes induced by a local Rayleigh-Taylor instability above the reaction zone and irregular fingering in the lower solution and plumes on top induced by differential diffusive effects. Unlike these cases, the pattern formation demonstrated in Eckert et al. (2004) strikes by its regularity.

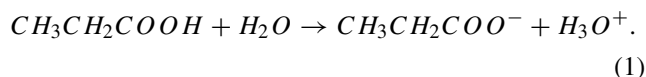
It was speculated that several mechanisms of hydrodynamic instability come into play in this case. In Bratsun and De Wit (2004), the partial role of the Marangoni instability in pattern formation was considered theoretically. It was found that a structure due to the combined effect of the reaction and Marangoni instability is unsteady and can exist for only a limited time. When the reaction front goes away from the interface, the Marangoni instability alone cannot sustain the structure any longer and it fades out. The effect of gravity as applied to the same system was explored in Bratsun and De Wit (2008, 2011). The focus of the work (Bratsun and De Wit 2011) was the development of the Rayleigh-Taylor instability, depending on the different values of the chemical reaction rate. The effect of heat in that paper was deliberately neglected from the outset. The paper (Bratsun and De Wit 2008) was devoted to external control of pattern formation in a Hele-Shaw reactor. It was shown that the Rayleigh-Taylor instability plays a key role in the formation of structures observed. However, the model proposed in Bratsun and De Wit (2008, 2011) could not explain fully the experiment (Eckert et al. 2004), since in numerical simulations the periodic structure of fingers was rather quickly destroyed after their formation. Thus, some unaccounted stabilizing mechanism obviously exists in the system.

As it is known, Rayleigh-Bénard convection is the instability of a fluid layer which is confined between two thermally conducting plates, and is heated from below to produce a fixed temperature difference. Since liquids typically have positive thermal expansion coefficient, the hot liquid at the bottom of the layer expands and produces an unstable density gradient. If the density gradient is sufficiently strong, the hot fluid will rise, causing a convective flow. If the layer is heated from above, the same mechanism acts trying to stabilize the layer since the cooler, denser liquid is already at the bottom. The purpose of the present work is to focus on the particular role of this Rayleigh-Bénard mechanism which should manifest itself clearly in the pattern formation during an exothermic reaction. We show that

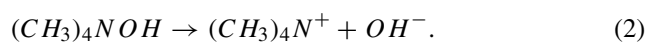
while the Rayleigh-Taylor instability acts as a main motor of the reactive fingering, the Rayleigh-Bénard mechanism associated with intensive heat release during the reaction may perform fine-tuning of the finger front.

### Theoretical Model

Let two immiscible liquids fill a Hele-Shaw cell. The upper layer is dilute acid solution in an organic solvent, and the lower layer is alkaline water. Carboxylic acids (acetic, formic, propionic) have been used in the experiments (Eckert et al. 2004). Tetra methyl ammonium hydroxide (TMAH) and some other substances have been used as a base. From a chemical kinetics perspective the system undergoes the following reactions. The acid permeating through the interface into the lower layer dissociates there disintegrating into hydronium cation and acid residue anion (as exemplified by propionic acid):



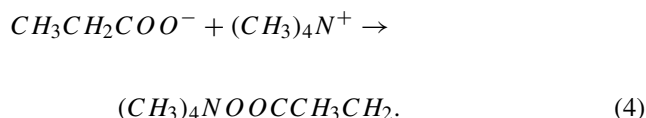
At the same time the dissociation process of TMAH base takes place in water, where the base disintegrates in the following way:



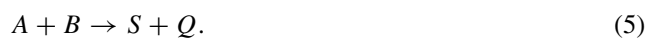
In aqueous solution cations  $H_3O^+$  find anions  $OH^-$  and form water:



At the same time the base cations find acid residue anions resulting in salt formation (methylammonium salt of propionic acid):



Thus, the neutralization reaction accompanied by significant heat release  $Q$  takes place in the lower layer. In (4) the reaction enthalpy is about  $-57 \text{ kJ/mol}$ . The chain of reactions (1–4) could be presented in simplified form:



It should be noted here that the reaction (5) is localized solely in the lower layer since TMAH and its salt do not dissolve in the upper layer. The system's non-autonomy is its another important peculiarity, as the reagents are not added during the reactions.

Let us outline the key assumptions, which have been taken into account in developing a theoretical model:

1. The gap  $h$  between the vertical plates is sufficiently small to consider the fluid flow as quasi-two-dimensional: the typical gap width of the cell in the experiment (Eckert and Grahn 1999) was 0.1 cm, while the height was more than two orders of magnitude;
2. The concentrations of chemical species are small enough (typically about 1 mol/l (Eckert et al. 2004)) so that the liquid's properties are independent on concentration;
3. The density of both liquids is equal to  $\rho$  (the density of the organic solvent in the upper layer is close to the value of the density of water);
4. All reagents have a similar diffusion coefficient  $D$ : this assumption is made in order to all the effects associated with a double-diffusion instability did not affect the results of this work;
5. Based on experimental observations in Eckert et al. (2004) we assume that the base  $B$  and salt  $S$  do not dissolve in the upper layer: the reaction takes place solely in the lower layer;
6. All phenomena connected with the surface tension are neglected in order to concentrate the attention to gravity-dependent phenomena. As it mentioned before, it was shown in Bratsun and De Wit (2004) that depending on the nature of reactants used, Marangoni effects due to surface tension gradients can come into effect as well. But the Marangoni instability is transient and can act for only a limited time since the reaction front gradually moves away from the interface. Moreover, the maximum value of the stream function for the flow induced by the pure Marangoni effect is approximately an order of magnitude less than in the case of the gravity-induced flow. Notice that by playing different organic reactants there is evidence that the use of organic reagents with longer chain allows for possible increased influence of their surface activity and even adsorption-desorption phenomena. In this paper, however, we consider acids with enough short chain to prevent these phenomena;
7. The interface remains plain and non-deformable, which is motivated by the experimental observations in a vertically oriented Hele-Shaw cell (Bratsun and De Wit 2004). In contrast to that, if the Hele-Shaw cell is tilted off the gravity, the instabilities in the system are characterized by the large scale interfacial deformation with a spatio-temporal periodicity together with the chemo-Marangoni convection (Shi and Eckert 2007);

8. Wide planes of a Hele-Shaw cell are considered thermally insulated until the contrary is not stated;
9. Initial concentrations of acid  $A_0$  and base  $B_0$  are equal;
10. The reaction rate  $k$  is fixed and equals to  $D/h^2 A_0$ .

The latter assumption means that the ratio of the chemical reaction rate to the diffusive mass transfer rate (the Damköhler number) is equal to 1. It is done to reduce the number of dimensionless parameters in the final equations and to focus on the effect under consideration. In fact, the possible variation of the Damköhler number can not affect the results qualitatively, as this variation can be accounted for changing the unit for temperature and rescaling of the thermal Rayleigh number.

Let us assume that coordinates  $x$  and  $z$  are drawn along the wide planes of a Hele-Shaw cell so that the line  $z = 0$  determines the surface between the layers. The cell boundaries are stated to be  $0 \leq x \leq H$ ,  $-L_b \leq z \leq L_u$ .

We choose the following units of measurement: length -  $h$ , time -  $h^2/D$ , velocity -  $D/h$ , temperature -  $QA_0/\rho C_p$ , pressure -  $\rho v_1 D/h^2$  and concentration -  $A_0$ . In what follows  $\eta_i$ ,  $\nu_i$ ,  $\kappa_i$ ,  $\chi_i$  define dynamic and kinematic viscosity, coefficients of thermal conductivity and temperature conductivity. The values with the index 1 and 2 refer to the lower and upper layers respectively. Then we shall get the convection-reaction-diffusion equations in a Hele-Shaw approximation for the lower layer:

$$\frac{1}{Sc} \left( \frac{\partial \Phi_1}{\partial t} + \frac{6}{5} \frac{\partial(\Psi_1, \Phi_1)}{\partial(z, x)} \right) = \Delta \Phi_1 - 12\Phi_1 + R \frac{\partial T_1}{\partial x} - R_A \frac{\partial A_1}{\partial x} - R_B \frac{\partial B_1}{\partial x} - R_S \frac{\partial S}{\partial x}, \quad (6)$$

$$\frac{\partial T_1}{\partial t} + \frac{\partial(\Psi_1, T_1)}{\partial(z, x)} = Le \Delta T_1 + A_1 B, \quad (7)$$

$$\frac{\partial A_1}{\partial t} + \frac{\partial(\Psi_1, A_1)}{\partial(z, x)} = \Delta A_1 - A_1 B, \quad (8)$$

$$\frac{\partial B}{\partial t} + \frac{\partial(\Psi_1, B)}{\partial(z, x)} = \Delta B - A_1 B, \quad (9)$$

$$\frac{\partial S}{\partial t} + \frac{\partial(\Psi_1, S)}{\partial(z, x)} = \Delta S + A_1 B \quad (10)$$

for the upper layer:

$$\frac{1}{Sc} \left( \frac{\partial \Phi_2}{\partial t} + \frac{6}{5} \frac{\partial(\Psi_2, \Phi_2)}{\partial(z, x)} \right) = \nu \Delta \Phi_2 - 12\nu \Phi_2 + Ra \frac{\partial T_2}{\partial x} - R_A \frac{\partial A_2}{\partial x}, \quad (11)$$

$$\frac{\partial T_2}{\partial t} + \frac{\partial(\Psi_2, T_2)}{\partial(z, x)} = \chi Le \Delta T_2, \quad (12)$$

$$\frac{\partial A_2}{\partial t} + \frac{\partial(\Psi_2, A_2)}{\partial(z, x)} = \Delta A_2, \quad (13)$$

Here we use a two-field formulation for movement equation, and we introduce the stream function  $\Psi$  and vorticity  $\Phi = -\Delta \Psi$ . The advection terms in (6–13) have been written in the compact form of the Jacobian determinant:

$$\frac{\partial(A, B)}{\partial(z, x)} = \frac{\partial A}{\partial z} \frac{\partial B}{\partial x} - \frac{\partial A}{\partial x} \frac{\partial B}{\partial z}.$$

The equations (6) and (11) differ from a standard Navier-Stokes equation by one more additional term linear in the vorticity. This term appearing within the Hele-Shaw approximation may be interpreted as the average friction force due to the presence of the plates and are analogous to the linear velocity term in Darcy's law valid for fluid flow in porous media. The equations (7) and (12) do not contain the analogous additives, as the vertical planes are considered to be thermally isolated.

One should provide boundary conditions to the equations (6–13):

$$z = -L_b : \quad \Psi_1 = 0, \quad \frac{\partial \Psi_1}{\partial z} = 0, \quad \frac{\partial T_1}{\partial z} = 0, \quad \frac{\partial A_1}{\partial z} = 0,$$

$$\frac{\partial B}{\partial z} = 0, \quad \frac{\partial S}{\partial z} = 0,$$

$$z = L_u : \quad \Psi_2 = 0, \quad \frac{\partial \Psi_2}{\partial z} = 0, \quad \frac{\partial T_2}{\partial z} = 0, \quad \frac{\partial A_2}{\partial z} = 0; \quad (14)$$

$$z = 0 : \quad \Psi_1 = 0, \quad \Psi_2 = 0, \quad \frac{\partial \Psi_1}{\partial z} = \frac{\partial \Psi_2}{\partial z}, \quad \Phi_1 = \eta \Phi_2,$$

$$T_1 = T_2, \quad \frac{\partial T_1}{\partial z} = \kappa \frac{\partial T_2}{\partial z}, \quad \frac{\partial S}{\partial z} = 0, \quad \frac{\partial B}{\partial z} = 0; \quad (15)$$

$$A_1 = A_2, \quad \frac{\partial A_1}{\partial z} = \kappa \frac{\partial A_2}{\partial z}$$

and the initial conditions at :

$$z < 0 : \quad \Psi_1 = 0, \quad \frac{\partial \Psi_1}{\partial z} = 0, \quad T_1 = 0, \quad A_1 = 0, \quad B = 1;$$

$$z > 0 : \quad \Psi_2 = 0, \quad \frac{\partial \Psi_2}{\partial z} = 0, \quad T_2 = 0, \quad A_2 = 1. \quad (16)$$

The full list of dimensionless parameters appeared in the system of equations (6–16) is given in the Table 1. As there are a lot of dimensionless parameters, a variety of phenomena described by the equations (6–16) is very wide. To focus on the effect of the heat release, we evaluated most of the parameters on the basis of the experimental data (Eckert et al. 2004). The Table 1 shows that Schmidt and Lewis numbers representing the relations of characteristic time of acid diffusion to the characteristic values of hydrodynamic and thermal time equal to  $Sc = 980$  and  $Le = 130$ , respectively. This means that the diffusion processes of reagents are significantly slower than other diffusion processes in the system. Therefore the diffusion processes determine nonlin-

**Table 1** List of dimensionless parameters

Definition	Name of the parameter
$Sc = \nu_1/D$	Schmidt number
$Le = \chi_1/D$	Lewis number
$R = g\beta_T Q A_0 \chi_1 h^3 / D \kappa_1 \nu_1$	Rayleigh number for heat
$R_A = g\beta_A A_0 h^3 / D \nu_1$	Rayleigh number for acid
$R_B = g\beta_B A_0 h^3 / D \nu_1$	Rayleigh number for base
$R_S = g\beta_S A_0 h^3 / D \nu_1$	Rayleigh number for salt
$\kappa = \kappa_2/\kappa_1$	heat conductivity ratio
$\chi = \chi_2/\chi_1$	heat diffusivity ratio
$\nu = \nu_2/\nu_1$	kinematic viscosity ratio
$\eta = \eta_2/\eta_1$	dynamic viscosity ratio

ear dynamics of the system. Values for the solutal Rayleigh number for the propionic acid ( $CH_3CH_2COOH$ ), TMAH ( $(CH_3)_4NOH$ ) and their salt appear to be equal to  $R_A = 2200$ ,  $R_B = 1800$ ,  $R_S = 1100$  (Bratsun and De Wit 2008). Thus, thermal Rayleigh number  $R$  is the only parameter left undefined. Since the configuration of more dense acid on top of less dense base ( $R_A > R_B$ ) is unstable in the presence of gravity one can expect the development of the Rayleigh-Taylor instability which is usually accompanied by density-driven fingering with the irregular behavior of the downward front.

**Base State**

Let us assume that the fluid is at rest in both layers. The system of equations (6–16) allows for an important class of non-steady solutions, which describe the dynamics of the reaction-diffusion processes. Let us term this system state as the base state. Then we consider the concentration and temperature fields depending from the vertical axis solely:  $T_i^0(t, z)$ ,  $A_i^0(t, z)$ ,  $B^0(t, z)$ ,  $S^0(t, z)$ . Then we get:

$$\begin{aligned} \frac{\partial T_1^0}{\partial t} &= Le \frac{\partial^2 T_1^0}{\partial z^2} + A_1^0 B^0, & \frac{\partial T_1^0}{\partial t} &= \chi Le \frac{\partial^2 T_2^0}{\partial z^2}, \\ \frac{\partial A_1^0}{\partial t} &= \frac{\partial^2 A_1^0}{\partial z^2} - A_1^0 B^0, & \frac{\partial A_2^0}{\partial t} &= \frac{\partial^2 A_2^0}{\partial z^2}, \\ \frac{\partial B^0}{\partial t} &= \frac{\partial^2 B^0}{\partial z^2} - A_1^0 B^0, & \frac{\partial S^0}{\partial t} &= \frac{\partial^2 S^0}{\partial z^2} + A_1^0 B^0, \end{aligned} \tag{17}$$

$$z = -L_b : T_1^0 = 0, \quad A_1^0 = 0, \quad B^0 = 1, \quad S^0 = 0, \tag{18}$$

$$z = L_u : T_2^0 = 0, \quad A_2^0 = 1, \tag{19}$$

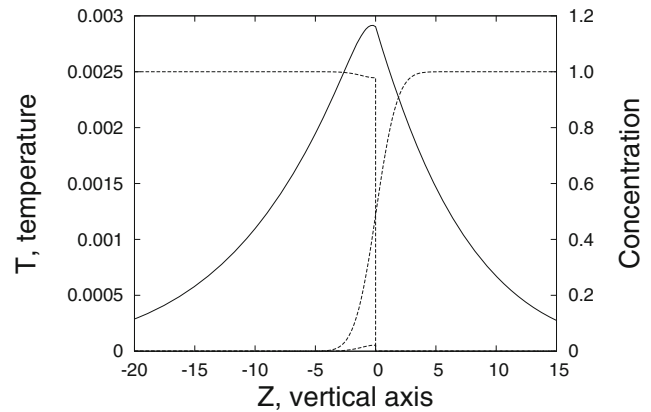


**Fig. 2** Temperature profile (solid line) and reagent concentration (dotted line) of the base reaction-diffusion state at  $t = 1$

$$\begin{aligned} z = 0 : T_1^0 &= T_2^0, & \frac{\partial T_1^0}{\partial z} &= \frac{\partial T_2^0}{\partial z}, & \frac{\partial B^0}{\partial z} &= 0, \\ A_1^0 &= A_2^0, & \frac{\partial A_1^0}{\partial z} &= \frac{\partial A_2^0}{\partial z}, & \frac{\partial S^0}{\partial z} &= 0. \end{aligned} \tag{20}$$

The problem (17–20) can be solved only numerically. The numerical method used for the integration (17–20) is analogous to the numerical method for the integration (6–16) and is discussed further. Figure 2 shows the profiles of reagents concentrations and temperature in a moment of time  $t = 1$ . A line in the space, where the concentrations of acid and base are the same, shall be designated as the reaction front. The front position is determined by the exact balance between diffusion-reaction processes, and its position in the space becomes quasi-steady at the equal reagent concentrations.

As we see from Fig. 1, the temperature curve has a local maximum. The existence of this maximum in the bulk can be evidenced analytically. Indeed, the temperature profile in the upper layer can be readily derived:

$$T_2^0(t, z) = \xi(t) \exp\left(-\sqrt{\frac{\alpha}{\chi Le}} z\right),$$

where  $\xi(t)$  denotes the temperature at the interface,  $\alpha$  is a positive constant. With boundary conditions (20) for a temperature gradient we get

$$\frac{\partial T_1^0}{\partial z} \Big|_{z=0} = -\frac{\kappa \xi(t) \sqrt{\alpha}}{\sqrt{\chi} Le}.$$

One can be clearly seen that the right part of this formula is always negative. By taking into account the boundary condition for the temperature (18), we can conclude that at least one maximum of the temperature profile should be placed between the interface  $z = 0$  and point  $z = -L_b$ . Our conclusion is supported by the numerical analysis (see Fig. 2). The location of the temperature maximum

is practically similar to the one of reaction front, because the maximal number of molecule pairs of acid and base is concentrated on the front line, thus emitting the maximum amount of heat.

Although the described process is simple in form, it results in a temperature gradient formation, which motivates the development of thermogravitational Rayleigh-Bénard instability in the area between the interface surface and reaction front (heating from below in the classic Rayleigh-Bénard problem) and suppression of the instability below reaction front (heating from above in the same problem). This is the peculiarity of the given system.

### Linear Stability Analysis

The next step in our analysis involves finding the conditions under which the reaction-diffusion non-stationary base state defined by (17–20) loses stability to give rise to convective solutions. To do so, we analyze the stability of the base state by linearizing the original system of equations (6–13) near it. We assume that small, monotonic disturbances periodic in the  $x$ -direction are superimposed upon the base state (17–20) in the following manner:

$$\begin{pmatrix} \Phi_i(t, x, z) \\ \Psi_i(t, x, z) \\ T_i(t, x, z) \\ A_i(t, x, z) \\ B(t, x, z) \\ S(t, x, z) \end{pmatrix} = \begin{pmatrix} 0 \\ 0 \\ T_i^0(t, z) \\ A_i^0(t, z) \\ B^0(t, z) \\ S^0(t, z) \end{pmatrix} + \begin{pmatrix} \varphi_i(t, z) \\ \psi_i(t, z) \\ \vartheta_i(t, z) \\ a_i(t, z) \\ b(t, z) \\ s(t, z) \end{pmatrix} e^{I k x}, \quad (21)$$

where  $\psi_i, \varphi_i, \vartheta_i, a_i, b, s$  are the amplitude of the disturbances of vorticity, the stream function, temperature, acid, base and salt concentrations respectively while  $k$  is their wavenumber.  $I$  is the imaginary unit.

By inserting the expansions (21) into the equations (6–13) and by linearising the latter near the base state, we obtain the following system of non-steady amplitude equations to define the critical disturbances:

$$\frac{1}{Sc} \frac{\partial \varphi_1}{\partial t} = \Delta \varphi_1 - 12 \varphi_1 - k^2 (R \vartheta_1 - R_A a_1 - R_B b - R_S s),$$

$$\frac{1}{Sc} \frac{\partial \varphi_2}{\partial t} = \nu \Delta \varphi_2 - 12 \nu \varphi_2 - k^2 (R \vartheta_2 - R_A a_2),$$

$$\frac{\partial \vartheta_1}{\partial t} = Le \Delta \vartheta_1 + A_1^0 b + B^0 a_1 + \psi_1 \frac{\partial T_1^0}{\partial z},$$

$$\frac{\partial \vartheta_2}{\partial t} = \chi Le \Delta \vartheta_2 + \psi_2 \frac{\partial T_2^0}{\partial z},$$

$$\frac{\partial a_1}{\partial t} = \Delta a_1 - A_1^0 b - B^0 a_1 + \psi_1 \frac{\partial A_1^0}{\partial z},$$

$$\frac{\partial a_2}{\partial t} = \Delta a_2 + \psi_2 \frac{\partial A_2^0}{\partial z},$$

$$\frac{\partial b}{\partial t} = \Delta b - A_1^0 b - B^0 a_1 + \psi_1 \frac{\partial B^0}{\partial z},$$

$$\frac{\partial s}{\partial t} = \Delta s + A_1^0 b + B^0 a_1 + \psi_1 \frac{\partial S^0}{\partial z}, \quad (22)$$

with boundary conditions:

$$z = -L_b : \varphi_1 = 0, \psi_1 = 0, \vartheta_1 = 0, a_1 = 0, b = 0, s = 0;$$

$$z = L_u : \varphi_2 = 0, \psi_2 = 0, \vartheta_2 = 0, a_2 = 0;$$

$$z = 0 : \varphi_1 = \eta \varphi_1, \psi_1 = \psi_2 = 0, \frac{\partial \psi_1}{\partial z} = \frac{\partial \psi_2}{\partial z}, \frac{\partial b}{\partial z} = 0,$$

$$\vartheta_1 = \vartheta_2, a_1 = a_2, \frac{\partial \vartheta_1}{\partial z} = \kappa \frac{\partial \vartheta_2}{\partial z}, \frac{\partial a_1}{\partial z} = \kappa \frac{\partial a_2}{\partial z}, \frac{\partial s}{\partial z} = 0.$$

Here:  $\Delta = \partial^2 / \partial z^2 - k^2$ .

The spectral amplitude problem involves both the equations to define the disturbances (22) and the equations system to define the base state (17–20). Nonsteady nature of the base state (17–20) and amplitudes is a feature of the problem obtained. The method of Initial Value Problem (IVP) suggested originally in Tan and Homsy (1986) has been used to solve the problem in this work. The method is a sort of Cauchy's problem - simple integrating of spectral amplitude equations for disturbances together with dynamically driven base state starting from some initial conditions. It was shown that the method gives adequate results, except for a short initial period of time, when the functions describing the base state are very quickly changed. In the case under analysis the initial time trouble resolves itself, as critically growing disturbances arise only after some time after the evolution begins, which is known to be longer the relaxation time in IVP method. More details about linear analysis in non-autonomous systems are given in papers (Bratsun and De Wit 2004; Tan and Homsy 1986).

In the problem (17–20) and (22) the acid is the disturbances generator, whereas the disturbances of velocity and temperature are "adjusted" to slowly developing disturbances of reagents concentrations due to large values of Schmidt and Lewis numbers. Thus, the increment  $\lambda$  is conveniently constructed through the disturbances of acid concentration:

$$\lambda(t) = \frac{1}{N} \sum_{j=1}^N \frac{1}{\Delta t} \ln \frac{a_{1j}(t + \Delta t)}{a_{1j}(t)}, \quad (23)$$

where  $\Delta t$  is the integration time step and  $N$  is the number of independent realizations (typically  $N$  is equal to 10–15).

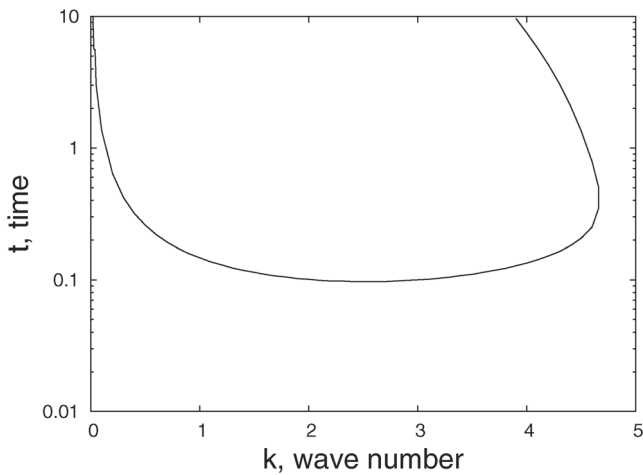


**Fig. 3** Neutral curve for the Rayleigh-Taylor instability at  $R = 500$ . Time axis is shown in a logarithmic scale

It should be noted that the expression (23) has been written similarly to a Lyapunov exponent. Because the growth rate  $\lambda$  is sensitive to the given initial data, each independent integration starts from white noise with an amplitude less than  $10^{-4}$ . We have fixed the occurrence of instability to the time when  $\lambda(t)$  averaged over several realizations changes sign from negative to positive. The start of instability (or exit from it) is fixed at the moment of the change of increment sign (23), averaged by the number of independent realizations  $N$ .

Figure 3 shows the neutral curve for the Rayleigh-Taylor instability obtained in the frame of the linear analysis for  $R = 500$ . As the system is non-autonomous, the time serves as a problem parameter here. The Figure illustrates that all modes are steady at the very beginning of the evolution. In a moment of time  $t \approx 0.1$  disturbance with a wave number  $k \approx 2.6$  is the first to lose stability. Then more and more waves are involved into the instability area. One can see that the Rayleigh-Taylor instability (inside the area limited by loop in the Fig. 3) includes a wide spectrum of wavelengths. We found that the wave number of the structure slightly decreases with time. This occurs because the maximum growth rate of perturbations in the region of instability is shifted towards longer wavelengths.

**Numerical Method for Fully Non-Linear Problem**

The problem (6–16) has been solved numerically by a finite-difference method. A detailed description of the method is given in our previous paper (Bratsun and De Wit 2011). The numerical scheme we use is a scheme proposed in Simanovskii and Nepomnyashchy (1993). An explicit

scheme has been used, and in order to ensure the stability of the method, the time step was calculated by the formula

$$\Delta t = \frac{\Delta x^2}{2(2 + \max(|\Psi_i|, |\Phi_i|))}$$

The Poisson equations are solved by the iterative Liebmann successive over-relaxation method at each time step: the accuracy of the solution is fixed to  $10^{-4}$ . At the interface the vorticity was calculated by the formula suggested in Simanovskii and Nepomnyashchy (1993):

$$\Phi_2(x, 0) = -\frac{2(\Psi_1(x, -\Delta z) + \Psi_2(x, \Delta z))}{\Delta z^2(1 + \eta)}$$

$$\Phi_1(x, 0) = \eta\Phi_2(x, 0)$$

Here  $\Delta x, \Delta z$  is a mesh size for the corresponding horizontal and vertical coordinates. We have generalized the numerical scheme by considering additional concentration fields for the reacting chemical species. The acid concentration at the interface was calculated by the second-order approximation formula:

$$A_1(x, 0) = A_2(x, 0) = \frac{1}{6}(4A_1(x, -\Delta z) -$$

$$A_1(x, -2\Delta z) + 4A_2(x, \Delta z) - A_2(x, 2\Delta z))$$

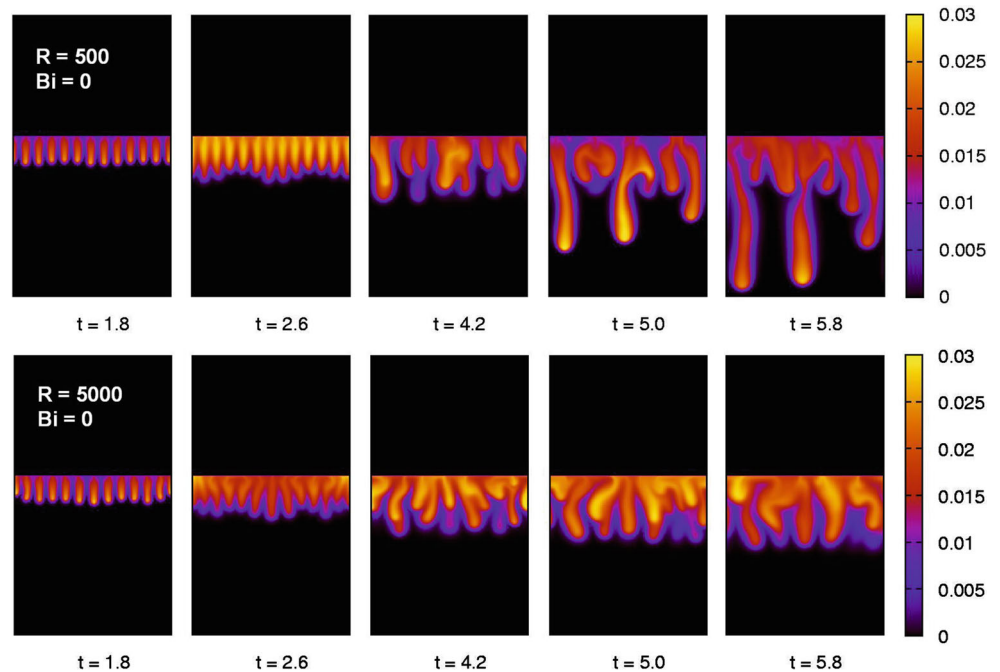
For all fields at the vertical boundaries  $x = 0, H$  we apply periodic boundary conditions. In most calculations we define the area as  $H = 40, L_u = 30, L_b = 40$ . We perform the calculations at uniform rectangular mesh 200 by 350. As the initial condition we use a random distribution of the stream function field with amplitude less than  $10^{-3}$ .

It is known that a chemical reaction and convection may interact in following way: if reaction influences the convection’s intensity via the formation of light (or heavy) salt and heat release, the convective flow significantly affects the reaction rate, thus ensuring more intensive mixing of the reacting substances. That is why the following integral characteristic gives valuable information:

$$Re(t) = \frac{1}{HL_b} \int_{-L_b}^0 \int_0^H \zeta(t, x, z) dx dz,$$

where field  $\zeta = 1$  in all cases, when the salt concentration is above some limit  $S(t, x, z) > S^*$ , and zero in all other points in the area. The threshold  $S^*$  is a small, arbitrary value. Since typical values of the salt concentration in the problem does not exceed 0.1 (see Fig. 4), we define this limit as  $S^* = 10^{-3}$ . Thus, value  $Re(t)$  may be interpreted as the time-dependent reaction rate computed in terms of the area of the reacted zone normalized by the width of the system.

**Fig. 4** Non-linear evolution of the salt concentration from an initially perturbed base state to a fingering pattern for  $R = 500$  (upper row) and  $R = 5000$  (lower row). The frames pertain to times  $t = 1.8, 2.6, 4.2, 5.0, 5.8$  respectively. The drastic change in the evolution of the system is reflected in the reaction rate  $Re(t)$  variation in time shown in Fig. 5



## Results of Numerical Simulation

A levelling effect of the Rayleigh-Bénard mechanism on the envelope of the chemoconvective structures is clearly seen in Fig. 4, where the frames of the evolution of salt concentration field  $S$  for five successive times for the cases  $R = 500$  and  $R = 5000$ , respectively, are presented. The graph of integral reaction rate  $Re(t)$  as a time function is shown in Fig. 5.

First, let us look at the case  $R = 500$ . We should note here that the time in this problem may be considered as a bifurcation parameter, because the pattern formation conditions dynamically change. The process of pattern formation in a system undergoes, at least, four stages of development. The first stage  $0 < t < 1.4$  is characterized by the development of the pure diffusive scenario with no convection taking place (Fig. 2). The acid penetrates in the lower layer through the free surface and enters in the reaction with alkali there. Due to diffusion the reaction zone advances according to a root law (Fig. 5,  $R = 500$ ). At this stage nonsteady configuration is developed in the system: the gradient of acid concentration is directed upwards in both layers, thus arising the Rayleigh-Taylor instability. Although the gradient of the base in the lower layer is directed downwards, this stabilizing factor is balanced by the opposite gradient of salt, which is gradually accumulated in the system as a result of reaction. First, convection takes place in the upper layer, but starting from  $t \approx 1.4$  convection appears also in the lower one. As a result in the lower layer a regular structure of salt fingers is formed, reflecting the exact balance between the reaction, diffusion and convection (Fig. 4,  $t = 1.8$ ). This

structure consists of a periodic array of fingers elongating away from the free surface: the wave number is about 1.9 (12 fingers per 40 length units). This value is a bit lower than the critical wave number 2.6 at the minimum of the neutral curve at  $t = 0.1$  (Fig. 3). Since the problem is transient, the wave number of the structure slightly decreases with time. Thus, at this moment the curve of the salt fingers is a practically ideal straight line. But according to the diagram of the integral reaction rate (Fig. 5,  $R = 500$ ,  $t \approx 3$ ), the system is evolving again in accordance with diffusive scenario: the envelope is slowly moving away from the interface. However, the regular system of salt fingers eventually is destroyed - the envelope of the structure experiences a zigzag instability (Fig. 4,  $t = 2.6$ ). This is due to the acid inflow to the lower layer and accumulation of the reaction product. The Rayleigh-Taylor instability starts to prevail, and finally the front collapses by large salt fingers (Fig. 4,  $t = 5$ ). This immediately manifests itself in the intensification of the spatial reaction rate (Fig. 5,  $R = 500$ ,  $t > 4$ ).

The heat release plays a significant role in the envelope dynamics. Figure 2 shows that in the lower part of lower layer the temperature gradient is directed upwards, and the rate of fluid flow here abruptly decreases because of the Rayleigh-Bénard mechanism. The suppression of the vortex structures propagating large fingers down takes place at quite powerful heat field. When convection is suppressed the salt fingers diffuse and dissolve. The lower row in Fig. 5 presents evolution of salt field at more expressed thermal effect  $R = 5000$ . We can clearly see that the tips of all fingers are levelling at one line, even when the



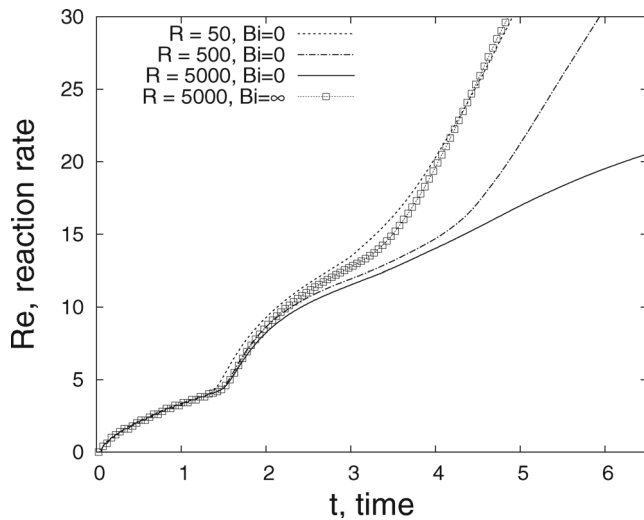


**Fig. 5** Numerical simulations of the integral reaction rate  $Re(t)$  as a function of time for different values of the Rayleigh number  $R = 50; 500; 5000$ . The Biot number is fixed to  $Bi = 0$  (lines) and  $Bi = \infty$  (squares)

dynamics of these chemoconvective structures are already chaotic (Fig. 4). At the same time the reaction rate grows linearly (Fig. 5,  $R = 5000, t > 3$ ), reflecting the fact of accurate balance between the reaction-diffusion and convection processes.

The numerical simulation for weaker thermal effect supports this conclusion - transfer to irregular distribution of large salt fingers takes place at the early stage of evolution (Fig. 5,  $R = 50$ ). Complete switching off of the thermal field immediately results in irregular density fingering.

### Effect of the Biot Number

As one can see from the definition of the thermal Rayleigh number (see Table 1), there is no physical value that would allow you to change easily this parameter during one series of experiments. The heat  $Q$  released during exothermic reaction creates the main effect. This value is determined by a combination of acid-base pairs and is fixed for a series of experiments with these reagents. On the other hand, the replacement of reagents changes both the value of the thermal Rayleigh number  $R$  and solutal Rayleigh numbers  $R_A, R_B, R_S$ .

For experimental verification of the effect one can act differently. In order to weaken the effect of the thermogravitational mechanism one can remove the heat through the wide planes of a Hele-Shaw cell. It can be done by changing the thermal conductive properties of the planes by means of placing them in close contact with a highly thermal conductive body. In this case the heat is rather dissipated through the wide place, than accumulates and diffuses along the layer. It means that the effective value of the Rayleigh

number decreases sharply. The experiments with local cooling of the reactor’s walls carried out in Bratsun et al. (2005) indirectly support the conclusion of this paper about the effect of self-alignment of the envelope of the finger structures by the intensive thermal field: if we remove the heat from a Hele-Shaw reactor, there immediately appeared irregular fingering characterized by the chaotic propagation of the large salt fingers under strong Rayleigh-Taylor instability.

To illustrate this effect numerically we introduce the new parameter:

$$Bi = \frac{h\gamma_T}{2\kappa_1} \tag{24}$$

The dimensionless Biot number  $Bi$  is defined by (24), where  $\gamma_T$  is the heat exchange coefficient between the fluid and the solid walls and  $\kappa_1$  is the coefficient of thermal conductivity of water in the lower layer. Depending on the plates composition and their thickness  $l$ , the Biot number  $Bi$  may take a value from 0 to  $\infty$ . Taking into account this effect, the energy equation (7, 12) can be rewritten respectively as follows:

$$\begin{aligned} \frac{\partial T_1}{\partial t} + \frac{3(5+2Bi)}{5(3+Bi)} \frac{\partial(\Psi_1, T_1)}{\partial(z, x)} = \\ = Le\Delta T_1 - Le \frac{12Bi}{3+Bi} T_1 + A_1 B, \end{aligned} \tag{25}$$

$$\begin{aligned} \frac{\partial T_2}{\partial t} + \frac{3(5+2Bi)}{5(3+Bi)} \frac{\partial(\Psi_2, T_2)}{\partial(z, x)} = \\ = \chi Le\Delta T_1 - \chi Le \frac{12Bi}{3+Bi} T_2, \end{aligned} \tag{26}$$

Similarly to motion equations (6) and (11), heat equations (25) and (26) differ from a standard heat equation by the additional Darcy-like term in the right hand part. This term relates to the process of dissipation of heat through the solid plates. The difference with the Darcy term in (6–11) is that this term vanishes if the plates are made from thermoisolated material for which  $Bi = 0$ . If the plates are highly conductive, the dissipation rate is maximal and  $Bi = \infty$ . Comparing the equations (7, 12) with (25, 26) one can see that from the very beginning we have assumed that the dissipation of heat through the sidewalls is missing  $Bi = 0$ . It was done in order to maximize the effect of alignment of salt fingers on which we focus in this paper.

We can estimate the Biot number for a typical experimental setup (for example, as in Eckert and Grahn 1999; Eckert et al. 2004). The heat exchange coefficient  $\gamma_T$  may be estimated as  $\gamma_T \approx \kappa_s/l$ , where  $\kappa_s$  is the thermal conductivity of the solid plates and  $l$  is their thickness. Taking into account that  $l \approx h/2$  and that plates are made of glass, the conductivity of which is close to the conductivity of water filling

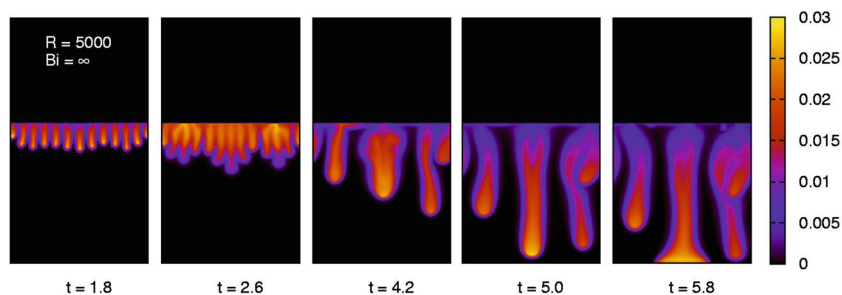


**Fig. 6** Non-linear evolution of the salt concentration from an initially perturbed base state to a fingering pattern for  $R = 5000$  and  $Bi = \infty$ . The frames pertain to times  $t = 1.8, 2.6, 4.2, 5.0, 5.8$  respectively. The Biot number effect manifests itself in the appearance of irregular

density-driven fingering (compare with Fig. 4, lower row). The corresponding reaction rate  $Re(t)$  variation in time is indicated in Fig. 5 by squares

the lower layer where the reaction occurs, we obtain  $Bi \sim 1$ , which means that heat dissipation during the experiment is quite intensive.

The effect of high-conductivity of the Hele-Shaw cell sidewalls is clearly seen in Fig. 6, where the frames of the evolution of salt concentration field  $S$  for five successive times for the case  $R = 5000$  and  $Bi = \infty$  are presented. Numerical simulation was made for the same parameter values as in the case shown in Fig. 4 ( $R = 5000$ , lower row). If the heat is dissipated through the lateral boundaries, the deterring effect via Rayleigh-Bénard mechanism disappears, and there comes a time for disordered fingering due to the uncompensated Rayleigh-Taylor instability. The drastic change in the evolution of the same system for two different Biot number is reflected also in the reaction rate  $Re(t)$  variation in time shown in Fig. 5. The cases  $Bi = 0$  and  $Bi = \infty$  are indicated by the solid line and squares respectively.

## Conclusions

In immiscible two-layer systems oriented vertically in the gravity field, convection can set in upon diffusion of a chemical species  $A$  from the upper to the lower layer where a species  $B$  is initially dissolved. The purpose of the present work is to focus on the particular role of thermal effect manifesting itself clearly in the pattern formation during exothermic reaction  $A + B \rightarrow S$  taking place solely in the lower layer. We have shown that while the Rayleigh-Taylor instability acts as a main motor of the reactive fingering, the Rayleigh-Bénard mechanism associated with intensive heat release during the reaction performs fine-tuning of the finger front. The maximum effect is observed when all the heat released during the reaction remains inside the Hele-Shaw cell. In the case of dissipation of heat through the wide sidewalls the effect of self-alignment of fingers envelope weakens or even disappears completely.

**Acknowledgements** We wish to thank K. Eckert and A. De Wit for stimulating discussions. The research has been carried out with the financial support from the Ministry of Education of Perm Region (grant C-26/244), Program of Strategic Development of Perm State Humanitarian Pedagogical University (project 031-F) and grants of Russian Fund for Basic Research (13-01-00508a, 14-01-96021r-ural\_a)

## References

- Almarcha, C., Trevelyan, P.M.J., Grosfils, P., De Wit, A.: Chemically Driven Hydrodynamic Instabilities. *Phys. Rev. Lett.* **044501**, 104 (2010)
- Almarcha, C., R'Honi, Y., De Decker, Y., Trevelyan, P.M.J., Eckert, K., De Wit, A.: Convective Mixing Induced by Acid-Base Reactions. *J. Phys. Chem. B* **115**, 9739–9744 (2011)
- Avnir, D., Kagan, M.L.: The Evolution of Chemical Patterns in Reactive Liquids Driven by Hydrodynamic Instabilities. *Chaos* **5**, 589601 (1995)
- Berg, J.C., Morig, C.R.: Density Effects in Interfacial Convection. *Chem. Eng. Sci.* **24**(6), 937–946 (1969)
- Bratsun, D.A., De Wit, A.: On Marangoni Convective Patterns Driven by an Exothermic Chemical Reaction in Two-Layer Systems. *Phys. Fluids* **16**(4), 1082–1096 (2004)
- Bratsun, D.A., De Wit, A.: Control of Chemoconvective Structures in a Slab Reactor. *Techn. Phys.* **53**, 146–153 (2008)
- Bratsun, D.A., De Wit, A.: Buoyancy-Driven Pattern Formation in Reactive Immiscible Two-Layer Systems. *Chem. Eng. Sci.* **66**(22), 5723–5734 (2011)
- Bratsun, D.A., Shi, Y., Eckert, K., De Wit, A.: Control of chemo-Hydrodynamic Pattern Formation by External Localized Cooling. *Europhys. Lett.* **69**(5), 746–752 (2005)
- De Wit, A.: Fingering of Chemical Fronts in Porous Media. *Phys. Rev. Lett.* **054502**, 87 (2001)
- Dupeyrat, M., Nakache, E.: Direct Conversion of Chemical Energy Into Mechanical Energy at an Oil Water Interface. *Bioelectrochem Bioenerg.* **5**, 134–141 (1978)
- Eckert, K., Grahn, A.: Plume and Finger Regimes Driven by a Exothermic Interfacial Reaction. *Phys. Rev. Lett.* **82**, 4436–4439 (1999)
- Eckert, K., Acker, M., Shi, Y.: Chemical Pattern Formation Driven by a Neutralization Reaction. Part I: Mechanism and Basic Features. *Phys. Fluids* **16**, 385–399 (2004)

- Nepomnyashchy, A., Simanovskii, I., Legros, J.C.: Interfacial Convection in Multilayer Systems, p. 498. Springer, New York (2012)
- Pons, A.J., Sagues, F., Bees, M.A., Sorensen, P.G.: Pattern Formation in the Methylene-Blue-Glucose System. *J. Phys. Chem. B* **104**, 22512259 (2000)
- Quincke, G.: Ueber Periodische Ausbreitung an Flüssigkeitsoberflächen und Dadurch Hervorgerufene Bewegungserscheinungen. *Ann. Phys. (Leipzig)* **35**, 580–642 (1888)
- Sherwood, T.S., Wei, J.C.: Interfacial Phenomena in Liquid Extraction. *Ind. Eng. Chem.* **49**, 1030–1034 (1957)
- Shi, Y., Eckert, K.: Orientation-Dependent Hydrodynamic Instabilities from Chemo-Marangoni Cells to Large Scale Interfacial Deformations. *Chin. J. Chem. Eng.* **15**, 748–753 (2007)
- Simanovskii, I.B., Nepomnyashchy, A.A.: Convective Instabilities in Systems with Interface, pp. 280, Gordon and Breach Science, Amsterdam (1993)
- Tan, C.T., Homsy, G.M.: Stability of Miscible Displacements in Porous Media: Rectilinear Ow. *Phys. Fluids* **29**, 3549–3557 (1986)
- Trevelyan, P.M.J., Almarcha, C., De Wit, A.: Buoyancy -Driven Instabilities of Miscible Two-Layer Stratifications in Porous Media and Hele-Shaw Cells. *J. Fluid Mech.* **670**, 3865 (2011)